The fusion of actin bundles driven by interacting motor proteins

2009 Phys. Biol. 6 036003

(http://iopscience.iop.org/1478-3975/6/3/036003)

Phys. Biol. **6** (2009) 036003 (10pp) doi:10.1088/1478-3975/6/3/036003

The fusion of actin bundles driven by interacting motor proteins

David Gillo[1,3], Barak Gilboa[1,2,3], Roi Gurka[1] and Anne Bernheim-Groswasser[1,4]

[1] Department of Chemical Engineering Ben-Gurion University of the Negev, PO Box 653, Beer-Sheva 84105, Israel
[2] Department of Physics, Ben-Gurion University of the Negev, PO Box 653, Beer-Sheva 84105, Israel

E-mail: bernheim@bgu.ac.il

Received 3 March 2009
Accepted for publication 25 March 2009
Published 1 May 2009
Online at stacks.iop.org/PhysBio/6/036003

Abstract
The cooperative action of many molecular motors is essential for dynamic processes such as cell motility and mitosis. This action can be studied by using motility assays which track the motion of cytoskeletal filaments over a surface coated with motor proteins. Here, we propose to use a motility assay consisting of a-polar actin bundles subjected to the action of myosin II motors where no external loading is applied. In this work we focus on those bundles undergoing fusion with other nearby bundles. Specifically, we investigate the role of the bundles' dimension on the transition from bidirectional to directional motion and on the properties of their motion during fusion. Our experimental data reveal that only small bundles exhibit dynamic transition to directional motion, implying that the forces acting on them exceed the threshold value necessary to induce the transition. Moreover, these bundles accelerate along their trajectory, suggesting that the forces acting on them increase while approaching each other. We show that these forces do not originate from external loading but rather arise from the action of the motors on the bundles. These forces are transmitted through the medium over micron-scale distances without being cut off. Moreover, we show that the forces propagate to distances that are proportional to the size of the bundles, or equivalently, to the number of motors, which they interact with.

M This article features online multimedia enhancements

S This article has associated online supplementary data files

1. Introduction

Many active processes in biological systems such as muscular contraction, cell motility and the organization and maintenance of a cytoskeletal structure are mediated by molecular motors. These motors are protein molecules that hydrolyze adenosine triphosphate (ATP) to generate work and movement along cytoskeletal filaments, e.g. filamentous actin (F-actin) and microtubules (MT) [1]. Different families of motor proteins have been distinguished. Dyneins and kinesins move along MT, while myosins walk along actin filaments. A given type of motor has a particular directionality of motion along its polar track filament [2–5]. Some motors move toward the 'plus' end of their track filaments, e.g. conventional kinesins and myosin II move toward the 'plus' ends of MT and actin filaments, respectively. Others move in the opposite direction such as Ncd, a kinesin-related motor of *Drosophila* which moves toward the 'minus' end of MT [6]. Recently, it was shown that NK11, a Ncd mutant, which differs from Ncd in only one amino acid (aa) in the neck region, apparently lacks a well-defined directionality as an individual motor [7].

Motor proteins can work as individual force-generating elements, for example, when transporting cargoes from one part of the cell to the other [1]. However, in many cellular

[3] These authors contributed equally to the work.
[4] Author to whom correspondence should be addressed.

processes, motors do not operate as single elements; rather, they work cooperatively. For example, to control the self-organization and dynamics of various cellular sub-structures, such as the formation of a contractile ring during the last step of cell division [8], stress fibers [9] and mitotic spindle assembly [10]. In addition, cooperative behaviors of groups of motors in many active processes in biological systems are at the origin of different types of dynamic instabilities. Collective effects are likely to occur in the actin–myosin system where they could be the key for understanding the oscillatory movement of myofibrils [11] and insect flight muscles [12]. Moreover, dynamic instabilities resulting from collective effects of dynein motors could be the origin of the oscillatory motion of axonemal cilia and flagella [13, 14]. These are also suggested to be the source of the ability of auditory hair cells to detect and amplify minute auditory stimuli [15–17].

The directionality of individual motors stems from interactions between different parts of the motor and from interactions between the motor and the track filament [18, 19]. The direction of motion of a large collection of motors may also be influenced by their cooperative mode of action. Specifically, in several recent experiments the ability of motors to cooperatively induce bidirectional motion has been demonstrated [20–22]. In one such experiment, we have investigated the motion of globally a-polar actin bundles, generated from severed (polar) actin filament fragments which are randomly recombined, and subjected to the action of a 'bed' of myosin II motors [22]. These a-polar bundles exhibit two significant dynamic behaviors. The majority move in a persistent bidirectional manner ('back and forth' motion) throughout the overall time of the experiment, exhibiting characteristic reversal times in the range of $\tau_{\mathrm{rev}} \sim 3$–$10$ s. We have found that these reversal times show no apparent correlation with the size of the gliding bundles, or equivalently, with the number of interacting motors, N [22]. Some of these bundles undergo a dynamic transition of their mode of motion, changing from bidirectional to directional motion, and fuse with nearby bundles.

In this work, we focus on those bundles undergoing fusion with nearby bundles. Specifically, we investigate the role of the bundles' dimension on the transition from bidirectional to directional motion and on the properties of their motion during fusion. Our experimental data reveal that only small bundles exhibit dynamic transition to directional motion, implying that the forces acting on them exceed the threshold value necessary to induce the transition. Moreover, these bundles accelerate along their trajectory, suggesting that the forces acting on them increase while the two bundles are approaching each other. Previous studies have shown that dynamic transitions from bidirectional to directional motion can be induced by the application of external forces or loads [23–26]. We show that the forces developed in the system do not result from the application of external loading, but rather, originate from forces generated by the myosin II motors acting on the actin filaments/bundles. These forces are transmitted through the system over micron-scale distances without being cut off. Moreover, we show that the forces propagate to distances which are proportional to the size of the bundles, or equivalently, to the number of motors N_s, which they interact with.

2. Materials and methods

Protein purification. Actin is purified from rabbit skeletal muscle acetone powder [27]. Purification of myosin II skeletal muscle is done according to standard protocols [28]. Actin labeled on Cys374 with Oregon Green (OG) purchased from Invitrogen.

NEM myosin II. *N*-Ethylmaleimide (Sigma, Co.) inactivated myosin II is prepared according to the standard protocol kindly given by T D Pollard (Yale University).

Optical microscopy. Actin assembly was monitored for 30 min by fluorescence with an Olympus IX-71 microscope. The labeled actin (mole) fraction was 1/10 and the temperature at which the experiments were conducted was 23 °C. Time-laps images were acquired every 15 s using a DV-887 EMCCD camera (Andor Co., England).

2.1. Motility assay

Flow chamber preparation. In brief, two parafilm sheets are laid on a standard microscope slide at ∼2 mm distance. These are perpendicularly covered with a rectangular glass coverslip (figure 1(*a*)). In order to properly attach these together, the slide is heated on a standard laboratory heater which allows the parafilm to melt, gluing the pieces together. After cooling, the slide can be used for the experiment.

Assay protocol. Protocol for this assay was adopted from Kuhn *et al* [29]. The assay includes two essential steps: (a) immobilization of actin filaments on a bed of NEM myosin II inactivated motors, and (b) addition of active myosin II motors at a defined concentration. For that purpose, 7.5–8.5 μl of 0.2 μM NEM myosin II (prepared according to [29]) is introduced into a flow chamber (26 mm × 2 mm glass surface area) for 1 min of incubation followed by wash of the flow chamber with the BSA (bovine serum albumin) solution to passivate the surface. Following this, actin filaments are grown on the surface (3 μM 10% OG labeled; molar percentage). Finally, the cell is supplemented with 8 μl of 0.6 μM myosin II motors (in a 2× myosin solution containing 3.3 mM $MgCl_2$ 2 mM EGTA, 20 mM HEPES 1% methyl cellulose, 3.34 mM Mg-ATP, 400 mM DTT, 17.6 mM Dabco, pH = 7.6), 0.133M KCl, 5 μM vitamin-D and an ATP regenerating system containing 0.1 mg ml^{-1} creatine kinase (CK) and 1 mM creatine phosphate (CP)). At the KCl concentrations used in this assay, the myosin II motors are assembled in small motor aggregates (∼16 myosin II units/aggregate) also known as mini-filaments [30].

We estimate the motors' surface concentration c_m by assuming that all the motors that are introduced into the flow chamber adhere to the top and bottom glass surfaces of the flow cell (total surface, 104 mm^2). This gives $c_m \sim 27\,800\ (\mu\mathrm{m})^{-2}$, which corresponds to densely packed motor beds (typical distance of a few nanometers between motor heads). At such

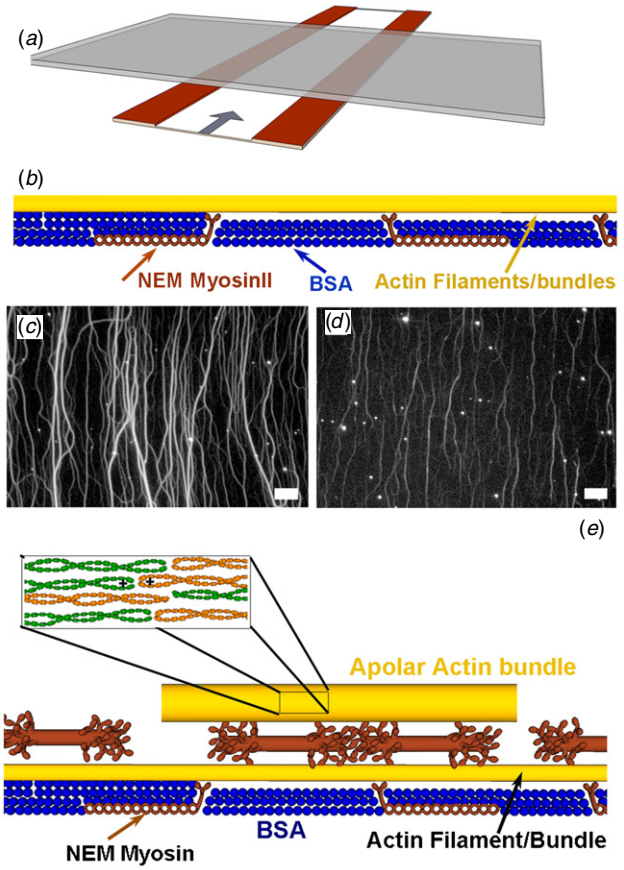

Figure 1. (*a*) Schematic drawing of the experimental flow chamber. Two parafilm sheets (brown) are laid on a standard microscope slide at an ∼2 mm distance. These are perpendicularly covered with a glass coverslip. In order to properly attach these together, the slide (upper grey surface) is heated on a standard laboratory heater which allows the parafilm to melt, gluing the pieces together. The arrow marks the place where solutions are inserted into the flow cell. (*b*) Schematic diagram of the system before the addition of active motors. The surface of a microscope slide was saturated by BSA (blue balls) and NEM myosin II (long, two-headed, brown objects). Actin filaments/bundles (thin yellow line) are attached to NEM myosin heads above the surface. (*c*), (*d*) Images of the system before the addition of active myosin II minifilaments. Image (*c*) shows the thick actin bundles formed at a high concentration of $MgCl_2$ (1.67 mM), while in (*d*) the thin bundles/filaments formed at a low $MgCl_2$ concentration (0.5 mM) are shown. Bar size is 5 μm. (*e*) After the initial step, myosin II minifilaments (multi-headed brown objects) were added to the cell sample. The motors that landed on the BSA surface created a homogenous 'bed' of immobile, yet active, motors. Other motors landed on the actin filaments/bundles (thin yellow line) present on the surface. The myosin II minifilaments started to move along the actin filaments/bundles. During their motion, the motors exerted forces on the actin filaments, which caused severing of small actin fragments. The ruptured actin fragments could move rapidly on the bed of active myosin II minifilaments and fuse with nearby or distant bundles. The bundles could further fuse with each other to form even larger, highly a-polar, bundles (thick yellow tube—the inset illustrates the internal structure of such a bundle, consisting of individual actin filaments with randomly orientated polarities).

high densities, inhomogenieties associated with the assembly of motors into mini-filaments can be ignored.

Data analysis. The position of fluorescent bundles is determined as the intensity center of mass using Metamorph (Molecular Devices) software. The position is analyzed using a custom MATLAB (The MathWorks, Inc.) program. The data is corrected for stage drift which is evaluated using immobile fluorescence spots present on the glass surface. The position of these spots is followed with time and fitted to a linear curve; this fit is further used to correct the motion of the bundles for stage drift.

Estimation of the bundles' dimension. We assume that the bundles are cylindrical; thus, their surface area is given by $A = 2\pi R_b L$, where R_b is the bundle radius and L is its length. The radius R_b of a bundle was estimated by dividing the integrated intensity measured perpendicular to the bundle $I_\perp$ by the intensity of single actin filaments I_f (measured independently on a solution of individual actin filaments under the same illuminating conditions). This gives an estimate for the number of filaments, N_f, composing the bundle. Assuming that the shape of the bundle is cylindrical, its radius can be estimated as $R_b = N_f^{0.5} r_f$, where $r_f = 3.75$ nm is the actin filament radius. Thus $A = 2\pi N_f^{0.5} r_f L = 2\pi \left(\frac{I_\perp}{I_f}\right)^{0.5} r_f L = \text{const}\left(I_N^{0.5} L\right)$ where $I_N = \frac{I_\perp}{I_f}$ is the normalized intensity.

Estimation of the number of interacting motors N. The motors are assumed to be distributed homogeneously on the slide and coverslip surfaces with a surface density c_m. The number of interacting motors N is given by $f c_m A = f c_m I_N^{0.5} L$, where f is a correction factor ($0 < f \leqslant 1$) that takes into account only the part of the bundle surface area and the motors that actually interact. (In practice, only the lower part of the bundles' surface area faces the motors; in addition, only the fraction of motors that face the bundle lower surface area have to be taken into account. These two contributions sum up in f.) Assuming that f is constant and independent of A, we find that the number of interacting motors N is proportional to surface area A (i.e. size) of the bundles.

Coarse grain analysis. In order to estimate the filaments' velocity, we utilize an image-processing algorithm that is based on the PIV (particle image velocimetry) technique. PIV is a well-known method which is used in fluid mechanics to measure the velocity field in a given flow. It is based on imaging the investigated flow and analyzing the images in order to obtain two-dimensional velocity maps. Each two consecutive images provide an instantaneous velocity field. Here, we utilize the same principle on the filament images using a freeware PIV algorithm [31]. Each image is divided to sub regions named 'interrogation window'. The size of the interrogation window was chosen to match the presence of a single actin bundle per window; therefore, correlated velocity represents the bundles' movement. The image analysis provides the average displacement of the bundle between two consecutive images. Since the time between images is known, a velocity value is calculated. A sub-pixel interpolation is used to obtain accurate velocity values (and not just discrete values). The results are filtered and erroneous vectors are removed. The

procedure of removing erroneous vectors includes two steps: global and local. The global filter calculates the mean of the whole vector map (300 vectors per map) and removes vectors which have a value greater or smaller than three standard deviation, i.e. $-3\sigma < v < +3\sigma$. This is followed by a local filter where each vector is compared to the median value of its vector neighbors, 5×5, and a threshold is applied; each vector would be in the range of ± 2 compared to the median. Once a vector is removed, an interpolation based on the neighbors is applied to replace the erroneous vector [31]. Based on the velocity fields, cross-correlation analysis for the lateral and longitudinal directions is performed: here we present the mathematical formulation for the cross-correlation analysis in the longitudinal direction:

$$VV_{\text{row}}(r) = \frac{1}{T \times M \times N} \times \sum_{k=1}^{T} \sum_{y=1}^{M} \sum_{x=1}^{N} V(x, y) \bullet V(x + r, y),$$

where V is the velocity component in the longitudinal direction, r is the distance where the correlation function is based upon, (x, y) are the longitudinal and lateral coordinates of the velocity, N is the number of velocity vectors in a row, M is the number of rows in the instantaneous vector map and T represents the number of vector maps. The procedure is repeated for the lateral directions:

$$VV_{\text{col}}(r) = \frac{1}{T \times N \times M} \times \sum_{k=1}^{T} \sum_{x=1}^{N} \sum_{y=1}^{M} V(x, y) \bullet V(x, y + r).$$

A characteristic result of the bundles' movement extracted using the PIV algorithm is given in figure S1 (available at stacks.iop.org/PhysBio/6/036003). The obtained velocity vectors represent the instantaneous movement of the actin bundles. Each vector was calculated based on a chosen interrogation window of size 64×64 pixels where the ratio of micron to pixel was equal to 0.26. The image size was 512×512 pixels, resulting in an average of 300 vectors per map. The same procedure was repeated for 106 consecutive images providing a statistical description of the filaments' dynamics.

3. Results

A diagrammatic representation of our experimental system is presented in figure 1. The protocol is based on that of Kuhn *et al* [29]. In brief, the surfaces of the flow chamber (figure 1(*a*)) was saturated with NEM-inactivated myosin II motors (drawn as long, two-headed, brown objects at the bottom of figure 1(*b*)) and passivated by BSA (blue balls in figure 1(*b*)). Subsequently, actin filaments/bundles (thin yellow line, figure 1(*b*)) were grown and held firmly on the NEM-myosin II bed. Figure 1(*c*) shows a characteristic fluorescent microscope image of the system which, at this stage, consisted of a large number of long actin bundles. The bundles were formed due to the presence of free Mg^{2+} ions (concentration 1.67 mM) and 0.5% methyl cellulose (MC). Free Mg^{2+} ions induced attractive electrostatic interactions between the actin filaments [32]. Unlike bundles formed by certain actin-binding proteins, filaments formed by condensation in the presence of multivalent cations are randomly arranged within the bundles without any specific polarity [33, 34]. MC can also induce the condensation of actin filaments into bundles [35]. However, as for the condensation induced by multivalent cations, in this case too, filaments within the bundles are expected to be randomly oriented without any specific polarity. At lower concentrations of Mg^{2+} (0.5 mM) (keeping the MC concentration fixed at 0.5%), both thinner bundles and single filaments were observed (figure 1(*d*)), suggesting that the Mg^{2+} ions were the prominent factor governing the condensation of actin filaments into bundles in this assay.

After growing bundles on the NEM-deactivated myosin II bed, we added active myosin II minifilaments (multi-headed brown objects, figure 1(*e*)) to the flow chamber. Motors which landed on the BSA surface created a homogenous 'bed' of immobile, yet active, motors. Other motors landed on the actin filaments/bundles present on the surface (figure 1(*c*)) and started to move along the actin tracks. In their motion the motors exerted forces on the actin filaments, leading to the severing of small actin filament fragments [22, 36, 37]. The ruptured actin fragments could move rapidly on the bed of active myosin II minifilaments and fuse with nearby or distant bundles. The bundles could further fuse with each other to form even larger, highly a-polar bundles (thick yellow tube—the inset illustrates the internal structure of such a bundle, consisting of individual actin filaments with randomly orientated polarities). The motion of most of the bundles shown in movie S1 (available at stacks.iop.org/PhysBio/6/036003) was bidirectional ('back and forth' motion). The motion took place both along pre-existing actin tracks and on the BSA bed, both of which were covered by active myosin II mini-filaments. (Uniform surface motor coverage motors were confirmed by experiments done at lower myosin II concentrations (0.3 μM). Under these conditions the bundles move directionally; their motion between these two areas was continuous, demonstrating that the whole surface was covered uniformly with motors [22].)

In some cases (~20% of the bundles), these a-polar bundles, that initially moved bidirectionally, suddenly underwent transition to directional motion, which was followed by their acceleration and fusion with a nearby bundle (see movie S1 available at stacks.iop.org/PhysBio/6/036003). Two such fusion events are presented in figure 2 (see also movie S2 available at stacks.iop.org/PhysBio/6/036003). Initially three different bundles (named '1' (pink), '2' (green) and '3' (yellow) in figure 2(*a*)) perform bidirectional motion independently (represented by the double headed arrows). The first to fuse were bundles '1' (pink) and '2' (green) (figures 2(*a*)–(*e*)). While bundle '1' moved bidirectionally during the overall fusion process, object '2', which is much shorter, showed a significantly different behavior. Initially, object '2' (green) moved bidirectionally up to a certain distance, D_f, from object '1' (pink). At this point, the movement of object '2' suddenly changed to directional, after

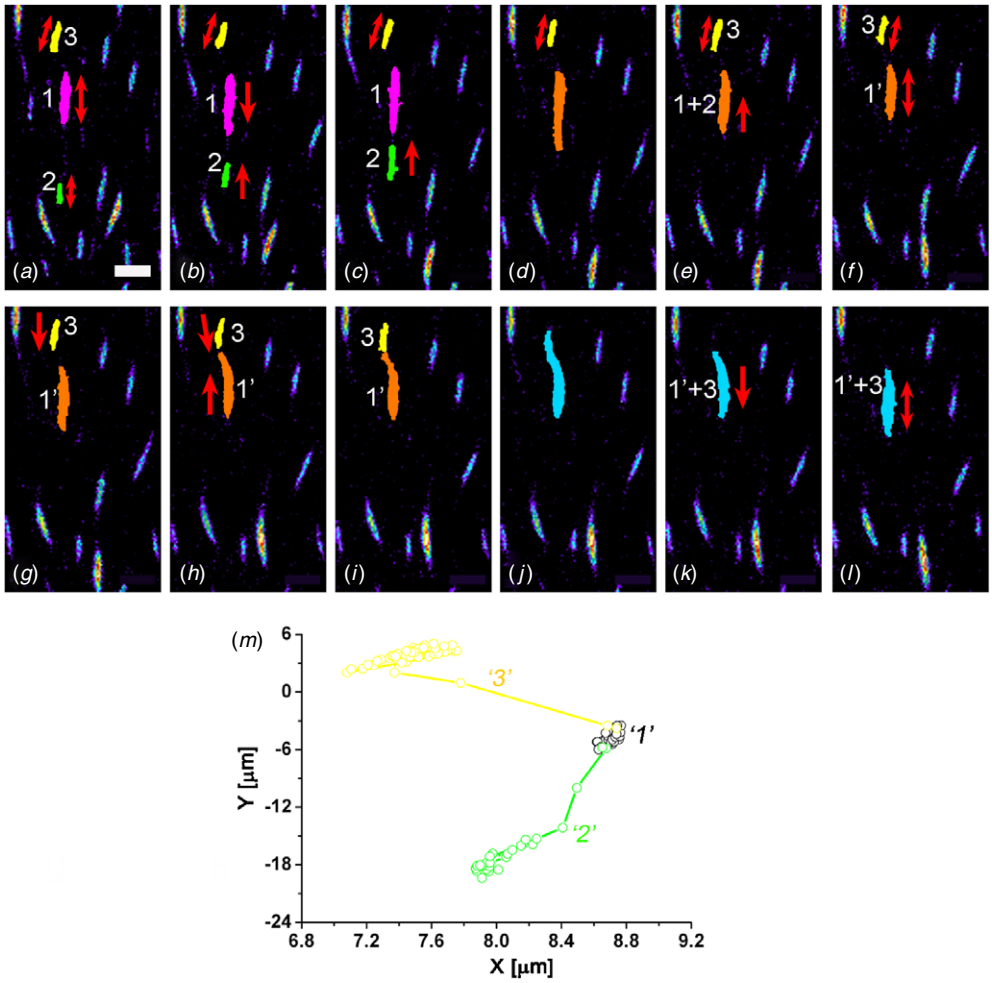

Figure 2. Transition from bidirectional to directional motion and fusion of bundles. (*a*)–(*f*) The fusion process of two bundles, '1' and '2' (left to right). (*a*) Initially, bundles '1' (pink), '2' (green) and '3' (yellow) move bidirectionally (represented by double red arrows). Below a certain distance (*b*), bundle '2' motion shifts from bidirectional to directional until it fuses with object '1' ((*b*)–(*e*), directional motion is represented by the red arrows). (*f*) The fusion (between '1' and '2') generates a new bundle '1′' (orange) which moves bidirectionally (represented by a double red arrow). Next to the fuse are bundles '1′' and '3' ((*g*)–(*l*), left to right). Bundle '3' (yellow) starts moving directionally toward object '1′' (orange) (*g*)–(*j*) until fusion (*k*). After fusion, the new bundle (*l*) '1′' + '3' = '1‴' (blue) continues to move bidirectionally (bar = 5 μm). In (*m*) are given the positions of the center-of-mass of the three bundles in the *x*, *y* coordinates. The trajectory of object '1' is represented by the black curve, while the positions of objects '2' and '3' are represented by the green and yellow curves, respectively. Bundle '1' performs bidirectional movement during the overall time of the experiment (jerky black curve). Bundles '2' and '3' initially perform bidirectional motion (green and yellow curves, jerky part) which then transforms into directional motion (smooth region of the green and yellow curves).

which, it accelerated toward object '1' (directional motion is represented by the red arrows, figures 2(*b*)–(*e*)). During this process, actin filaments protruded from the object '1' core in the direction of object '2'. This extension became more and more significant the closer the two bundles got (see figures 2(*a*)–(*c*)). Eventually, the two bundles came into contact (figure 2(*d*)) and fused (figure 2(*e*)), creating a new (composite) bundle which recovered the object '1' initial shape (compare bundles '1' (pink) and '1′' (orange) in figures 2(*a*) and (*f*)), and similar to bundle '1', bundle '1′' also moved bidirectionally (orange object in figure 2(*f*); as before, bidirectional motion is represented by the double headed arrow).

The next to fuse were objects '3' (yellow) and '1′' (orange) (figures 2(*g*), (*k*)). Here we saw a very similar behavior with object '1′' continuing to perform bidirectional motion while object '3' (yellow) suddenly changed its mode of motion from bidirectional (figure 2(*f*)), to directional (figures 2(*g*)–(*j*)) till fusion (figure 2(*k*)). The outcome of this fusion was the formation of a new composite bundle ('1′' + '3' = '1‴' (blue)) performing bidirectional motion (double headed arrow in figure 2(*l*)). The positions of center-of-mass of these three bundles in *x* and *y* coordinates through the entire process are depicted in figure 2(*m*).

Prior to fusion, the movement of the three bundles was bidirectional, i.e. the one-dimensional motion of the bundles did not persist in the initial direction, but rather exhibited frequent direction changes. The characteristic time between directional reversal τ_{rev} can be extracted by fitting the distribution of the reversal times with an exponential decay function. Measurements of the position of the center of mass and of the bundles' velocity exhibited a bimodal distribution

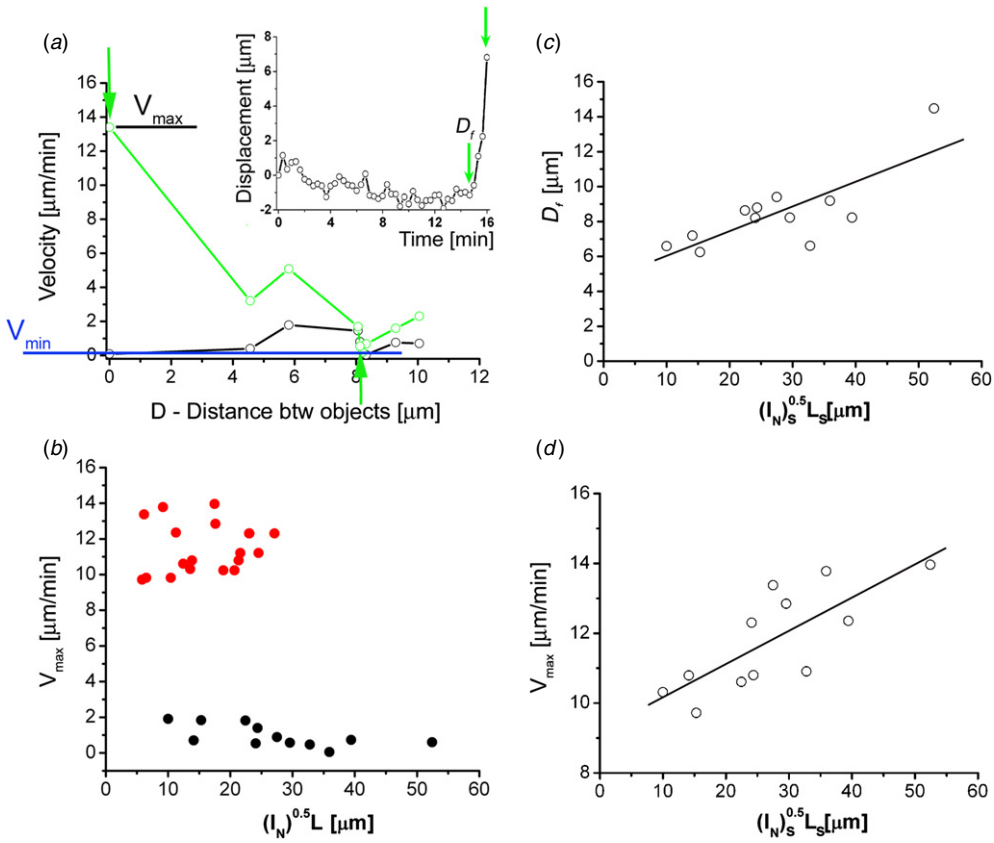

Figure 3. Dynamics of 'dynamic' and 'static' bundles. (*a*) Velocities of objects '1′' ('static' object) and '3' ('dynamic' object) during the fusion process are represented by the black and green curves, respectively. In both cases the velocity first decreases to a minimum value, $V_{\min}$, when the distance between the two bundles is D_f (marked by the lower green arrow). This step is followed by a sharp increase in the velocity of the 'dynamic' bundle (object '3' green curve) reaching a maximum value, $V_{\max}$, at fusion (the upper green arrow marks the fusion point). The inset shows the displacement of bundle '3' as a function of time; the fusion process is bounded by the two green arrows. (*b*) The terminal velocity, $V_{\max}$, as a function of the bundles' surface area, $I_N^{0.5}L$. Black symbols represent 'static' bundles while red symbols represent 'dynamic' bundles. (*c*) The distance to fusion, D_f as a function of the size (i.e. area) of the 'static' bundles, $I_{N,s}^{0.5}L_s$. The distance D_f increases linearly with $I_{N,s}^{0.5}L_s$ (see linear fit—black line). (*d*) The terminal velocity, $V_{\max}$, of the 'dynamic' bundles, as a function of $I_{N,s}^{0.5}L_s$. The two variables are linearly correlated (see fit—black line).

indicative of bidirectional motion (data not shown; see also [22]). The average speed of the motion, to the left or to the right was similar $|v_b| \sim$1–2 μm min^{-1}, which is two orders of magnitude lower than the velocities measured in gliding assays of polar actin filaments on myosin II motors [38]. The fact that the typical speed of the bidirectional motion is considerably smaller than those of directionally moving polar actin filaments can be partially attributed to the action of individual motors working against each other in opposite directions. We did not observe any significant changes in the velocity histogram of object '1' after the two consecutive fusion events it underwent, suggesting that its internal organization was globally unaffected and remained overall a-polar.

Next, we analyzed the motion of the bundles from the transition point until their final fusion, by plotting their velocity as a function of the inter bundle distance, D. In figure 3(*a*), the velocities of bundles '1′' (black curve) and '3' (green curve) are given. The dynamics of these bundles are representative of all other bundles whose motion we analyzed. Initially, we observe a decrease in the velocity of the bundles until $V_{\min} \sim 0.2$ μm min^{-1} (i.e. nearly stall), when approaching an inter-bundle distance, D_f, $\sim$ 8 μm (figure 3(*a*)). We define the length D_f as the characteristic 'distance to fusion' which corresponds to the distance between the two bundles' centers-of-mass at $V_{\min}$. This step is followed by a sharp increase in the velocity of the smaller bundle, i.e. object '3' (green curve in figure 3(*a*)), reaching a maximal value $V_{\max} \sim 14$ μm min^{-1} at fusion, about two orders of magnitude larger than $V_{\min}$. In contrast to this, the speed of the larger bundle, i.e. object '1′' (black curve in figure 3(*a*)) barely changes during the fusion process.

Therefore, we distinguish between two types of bundles: (i) 'static' objects which are largely unaffected by the fusion process (figure 3(*b*), black dots), and (ii) 'dynamic' objects undergoing transition from bidirectional to directional movement, and experience a significant increase in their velocity (figure 3(*b*), red dots). Plotting the values of $V_{\max}$ for $\sim$30 bundles as a function of $I_N^{0.5}L$ (which correlates with the surface area, or equivalently, with the size of the bundle; see section 2) clearly shows that 'static' objects accumulate to low values of $V_{\max}$ with $\langle V_{\max} \rangle = 1.1 \pm 0.8$ (μm min^{-1})

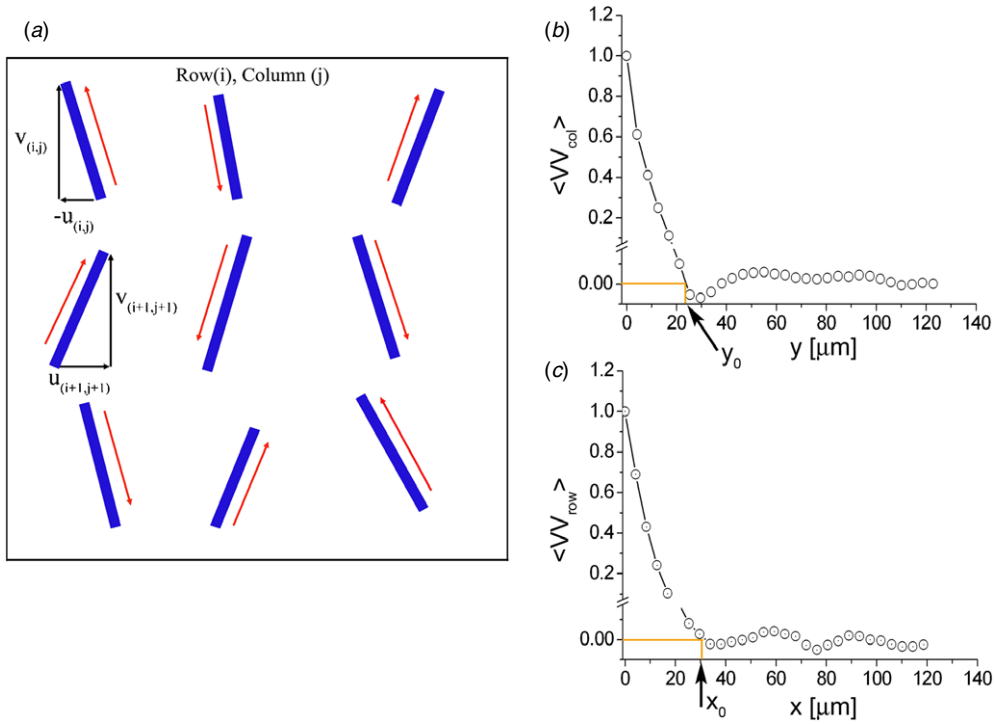

Figure 4. (*a*) Schematic representation of nine bundles in the velocity analysis output. The velocity of each bundle is represented by its position and velocity components. For example, a bundle in position i, j has lateral and longitudinal velocity components, $u_{i,j}$ and $v_{i,j}$, respectively. The velocity and its components are marked by the red and black arrows, respectively. (*b*), (*c*) Average velocity cross-correlation functions along columns and rows. The cross-correlation function was performed on each row and column for the velocity map and later on averaged on the entire set of vector maps. (*b*) The average cross-correlation of the longitudinal velocity component 'v' of bundles in the same column. (*c*) The average cross-correlation of the 'v' velocity component of bundles in the same row. Both figures have the same features in terms of values and profile behavior; crossing the zero around 25 μm (Y_0 and X_0 in (*b*) and (*c*), respectively) followed by an asymptotic line toward zero correlation values.

(average $\pm$ std) (note that $\langle V_{\max}\rangle \approx |v_b|$, the 'bidirectional' velocity, prior to fusion), and 'dynamic' objects which confine to higher values of $V_{\max}$ with $\langle V_{\max}\rangle = 11.4 \pm 1.4\,(\mu\text{m min}^{-1})$ (average $\pm$ std). Moreover, the 'dynamic' bundles concentrate to the region of small bundles in the diagram.

In many cases, fusion occurred between one 'static' and one 'dynamic' bundle. The data revealed that the distance to fusion, D_f, increased linearly with the size (i.e. surface area $I_{N,s}^{0.5}L_s$) of the attracting 'static' bundles (figure 3(*c*)), implying that larger bundles can transmit forces through the medium to longer distances. The size of the 'static' bundles also affects the velocity that the 'dynamic' bundles develop during the fusion process. We observe a linear correlation between the terminal velocity $V_{\max}$ of 'dynamic' bundles and the dimensions of the 'static' ones (figure 3(*d*)).

A conceptual view of the filaments' dynamic behavior is depicted in figure 4(*a*). The filaments instantaneously move in a longitudinal ('v') and lateral ('u') motion in a two-dimensional plane defined by the camera's axes. We analyzed the motion by using an experimental tool, originally designed for flow measurements, known as particle image velocimetry (PIV) [39]. The images were analyzed using cross-correlation function to obtain two-dimensional velocity fields [31] (see figure S1 in supplementary information available at stacks.iop.org/PhysBio/6/036003). A cross-correlation function has been applied to the velocity components in the longitudinal and lateral directions, respectively. The cross-correlation function was performed on each row and column for the velocity map and was later averaged over the entire set of vector maps. Figures 4(*b*) and (*c*) deduce the mean cross-correlation values for longitudinal velocity of the filaments in both directions. Both figures have the same features in terms of values and profile behavior; crossing zero at around 25 μm (Y_0 and X_0 in figures 4(*b*) and (*c*), respectively) followed by an asymptotic tendency toward zero correlation values. The point at which the correlation profile crosses zero can be referred to as the point where the two velocity vectors are not correlated beyond this distance for the calculated direction. Since the velocity vectors represent the bundles' movement, it is plausible to assume that at a distance of 25 μm and below, the bundles would be influenced from each other. The bundles' length is roughly 10 μm; thus one can argue that coupling between them occurs at distances which are at the same order of magnitude of their size.

4. Discussion

We have investigated the dynamics of myosin II motors on actin bundles composed of small filamentous segments with randomly alternating polarities. In this work we show that such a-polar actin bundles, initially moving bidirectionally, could suddenly change their regime of motion, from bidirectional to

directional, and fuse with other bundles located in their near proximity. This behavior has been shown to be significant throughout the analysis of our experiments. Previous studies have shown that dynamic transitions from bidirectional to directional motion can be induced by the application of external forces or loads [23–26]. In the current study, we do not apply any external forces to the system. However, some forces must exist in order to allow the dynamic phenomenon observed to occur. These forces are sufficient to induce the bundles to suddenly stop moving bidirectionally and start moving unidirectionally. Above this point, back reversal in the velocity mode is not observed; rather, unidirectional motion persists until the two bundles past each other and merge.

In this study we discriminate between two populations of bundles, 'static' and 'dynamic'. The velocity of 'static' bundles was barely affected by the fusion process and remained similar to its velocity prior to fusion ($\sim$1–2 μm min^{-1}). In contrast, 'dynamic' bundles underwent a dynamic transition which changed their motion into a directional one. Their velocity accelerated along their trajectory, up to a maximal velocity, $V_{\max}$, where fusion with a neighboring bundle occurred.

A detailed analysis demonstrates the presence of coupling between the terminal velocity ($V_{\max}$) of 'dynamic' fusing bundles and the 'size' of a corresponding 'static' attracting bundle. The linear correlation between the two variables (see figure 3(*d*)) suggests that the forces acting on a 'dynamic' bundle increase with the size (or surface area, $I_{N,s}^{0.5}L_s$) of the 'static' bundle, or equivalently, with the number of motors, N_s, that it is interacting with (see section 2). Moreover, we find that D_f is also linearly correlated with the bundles' size. Overall, our data shows that the 'attracting' forces propagate to longer distances D_f as $I_{N,s}^{0.5}L_s$ increases, implying that larger bundles influence their surrounding medium in a more important manner than smaller ones. To conclude, the size of the bundle, or equivalently, the number of interacting motors, N_s, as a parameter affects the system in the following manners:

(a) $V_{\max}$, the terminal velocity of the 'dynamic' bundles increases;
(b) the 'attracting' distance, D_f, increases;
(c) the 'static' bundles are less sensitive to forces imposed on them.

The analysis of the velocity cross-correlation provided scaling estimates to the dynamic behavior of the filaments. The analysis uses the full set of vector maps, providing a statistical significance to the obtained results. It was shown that the length scale of the phenomena is of the same order of magnitude as the size of the ('static') bundles themselves ($\sim$25 μm). Within this range of distances two bundles become correlated. We therefore suggest that the coupling between the two bundles happens within a distance which is comparable to the size of the larger one ('static'). The characteristic 'distance to fusion' D_f measured between 'static' and 'dynamic' bundles lies inside this range. However, D_f is a unique length scale since it points to the distance where the two bundles become strongly correlated and the forces that act between them reach a critical value. This distance corresponds to the point where the transition from bidirectional to directional motion occurs.

Our data reveal that the threshold force needed to induce the transition, from bidirectional to directional motion, is size dependent, i.e. the forces needed to drive the transition in small bundles are insufficient to provoke the same transition in large bundles. In the case of small bundles, the force exerted on the bundle distributes over a low number of motors (since the size of the bundles is proportional to N); thus, the force applied on each motor is larger, while the friction force is smaller (as the main contribution to the friction arise from motors that are interacting with the bundle) [22, 23, 40]. As a result, the applied forces are sufficient to induce transition from bidirectional to directional motion of small bundles, yet, they are below the threshold value in the case of large bundles.

The question is how long-range forces propagate through the system over micron-scale distances without being cut off. Both hydrodynamics and elasticity are potential candidates. In the latter case, the actin filaments/bundles that are attached to the glass surface serve as tracks over which the a-polar bundles are moving (on the bed of myosin II motors that landed on those tracks). The vibrating (i.e. bidirectionally moving) bundles exert elastic forces on the actin (gel-like) network in the surroundings. To the first order, the force distribution of each bundle can be represented by an anisotropic, force dipole. The interaction between two such active force dipoles [41] might play a role in initiating and directing the motion of the 'dynamic' objects, and pull the 'dynamic' bundles onto the 'right' track (i.e. on the actin track that connects the two bundles). Once pulled onto the right track, the 'dynamic' bundle accelerates toward the 'static' bundle. During this process, actin filaments were shown to protrude from the 'static' bundle core in the direction of the 'dynamic' bundle (figures 2(*b*), (*c*)), probably due to the pulling of actin filaments from the bundle core by myosin II motors present on the actin track (bed) in the vicinity of the bundles. The rapid extension of actin filaments near the bundle edges may also imply on a telescopic interaction between the filaments within the bundle, mediated by the myosin II motors [42, 43]. This would imply that myosin II motors are intercalated (i.e. 'sandwiched') inside the bundles' core (probably during the initial stage of their formation). Thus, when the two bundles approach, the protruding filaments may form new connections with myosin II motors residing in the other (nearby) bundle. Recent calculations demonstrate that interactions of filaments from two distinct bundles through the action of bipolar molecular motors can lead to the acceleration and fusion of the two bundles (personal communication, Assaf Zemel).

5. Conclusion and outlook

To conclude, in our system, the acceleration of the 'dynamic' bundles results from an increase in the overall attracting forces acting on it. The forces may be of multiple origins, i.e. external long-ranged (elastic and/or hydrodynamic origin) or internal short-ranged (resulting from interactions between individual actin filaments and motors from the two bundles) forces. These

may act simultaneously and contribute to the overall increase in velocity. Future work will test parameters not studied in this work. For instance, it will be of interest to label the myosin II motors in order to identify their surface coverage; this will be done by measuring the motors' local density on the BSA and actin bed. Moreover, it will enable determining whether motors are sandwiched within the bundles. This may explain (i) the protrusion of filaments from the bundle core when the two bundles approach each other, and (ii) the short-range attractions and eventual fusion of the two bundles. Furthermore, it will be important to investigate the origin of the long-ranged attractive forces, hydrodynamic versus elastic, and discriminate between the two possibilities; for example by varying the viscosity of the medium or the elastic properties of the surface. The latter can be done by varying the density of the actin filament bed. We hope that this study will stimulate theoretical work and efforts to better understand the mechanisms of acceleration and fusion.

Acknowledgments

We would like to thank Haim Diamant and Assaf Zemel for critical reading of the manuscript and useful discussions. We also thank Oded Farago and Oleg Krichevsky for useful discussions. This work was supported by the Reimund Stadler Minerva Center and by the research grants from the Israel Cancer Association (ICA grant 20070020B) and the Israel Science Foundation (ISF grant 551/04).

References

[1] Howard J 2001 *Mechanics of the Cell and the Cytoskeleton* (Sunderland, MA: Sinauer)
[2] Higuchi H and Endow S 2002 Directionality and processivity of molecular motors *Curr. Opin. Cell Biol.* **14** 50–7
[3] Höök P and Vallee R B 2006 The dyenin family at a glance *J. Cell Sci.* **119** 4369–71
[4] Block S 2007 Kinesin motor mechanics: binding, stepping, tracking, gating and limping *Biophys. J.* **92** 2986–95
[5] De La Cruz E M and Ostap E M 2004 Relating biochemistry and function in the myosin superfamily *Curr. Opin. Cell Biol.* **16** 61–7
[6] Sablin E P *et al* 1998 Direction determination in the minus-end-Directed kinesin motor NCD *Nature* **395** 813–6
[7] Higuchi H and Endow S A 2000 A mutant of the motor protein kinesin that moves in both directions on microtubules *Nature* **406** 913–6
[8] Reichl E M *et al* 2005 The stress and strain of cytokinesis *Trends Cell Biol.* **15** 200–6
[9] Hotulainen P and Lappalainen P 2006 Stress fibers are generated by two distinct actin assembly mechanisms in motile cells *J. Cell Biol.* **173** 383–94
[10] Robinson D C and Spudich J A 2000 Towards a molecular understanding of cytokinesis *Trends Cell Biol.* **10** 228–37
[11] Yasuda K *et al* 1996 Synchronous behavior of spontaneous oscillations of sarcomeres in skeletal myofibrils under isotonic conditions *Biophys J.* **70** 1823–9
[12] Pringle J W S 1977 *Insect Flight Muscle* ed R T Tregear (Amsterdam: North-Holland)
[13] Brokaw C J 1975 Molecular mechanism for oscillation in flagella and muscle *Proc. Natl Acad. Sci.* **72** 3102–6
[14] Camalet S *et al* 1999 Self-organized beating and swimming of internally driven filaments *Phys. Rev. Lett.* **82** 1590–3
[15] Martin P and Hudspeth A J 1999 Active hair bundle movement can amplify a hair cell's response to oscillatory mechanical stimuli *Proc. Natl Acad. Sci.* **96** 14306–11
[16] Camalet S *et al* 2000 Auditory sensitivity provided by self-tuned critical oscillations of hair cells *Proc. Natl Acad. Sci.* **97** 3183–8
[17] Eguiluz V M *et al* 2000 Essential nonlinearities in hearing *Phys. Rev. Lett.* **84** 5232–5
[18] Endow S A 1999 Determinants of molecular motor directionality *Nat. Cell Biol.* **1** 163–7
[19] Ménétry J *et al* 2005 The structure of the myosin VI motor reveals the mechanism of directionality reversal *Nature* **435** 779–85
[20] Endow S A and Higuchi H 2000 A mutant of the motor protein kinesin that moves in both directions on microtubules *Nature* **406** 913–6
[21] Tao L A *et al* 2006 A homotetrameric Kinesin-5, KLP61 F, bundles microtubules and antagonizes Ncd in motility assays *Curr. Biol.* **16** 2293–302
[22] Gilboa B *et al* 2009 Bidirectional cooperative motion of myosin-II motors on actin tracks with randomly alternating polarities *Soft Matter* at press doi:10.1039/b823400K
[23] Badoual M *et al* 2002 Bidirectional cooperative motion of molecular motors *Proc. Natl Acad. Sci.* **99** 6696–701
[24] Riveline D *et al* 1998 Acting on actin: the electric motility assay *Eur. Biophys. J.* **27** 403–8
[25] Jülicher F and Prost J 1995 Cooperative molecular motors *Phys. Rev. Lett.* **75** 2618–21
[26] Jülicher F and Prost J 1997 Spontaneous oscillations of collective molecular motors *Phys. Rev. Lett.* **78** 4510–3
[27] Spudich J A and Watt S 1971 The regulation of rabbit skeletal muscle contraction: I. Biochemical studies of the interaction of the tropomyosin-troponin complex with actin and the proteolytic fragments of myosin *J. Biol. Chem.* **246** 4866–71
[28] Margossian S S and Lowey S 1982 Preparation of myosin and its subfragments from rabbit skeletal muscle *Methods Enzymol.* **85** 55–71
[29] Kuhn J R and Pollard T D 2005 Real-time measurements of actin filament polymerization by total internal reflection fluorescence microscopy *Biophys. J.* **88** 1387–402
[30] Kaminer B and Bell A L 1966 Myosin filamentogenesis: effects of pH and ionic concentration *J. Mol. Biol.* **20** 391–4
[31] Gurka R *et al* 1999 Computation of pressure distribution using PIV velocity data *3rd Int. Workshop on PIV*
[32] Grazi E *et al* 1992 The control of cellular shape and motility. Magnesium and tropomyosin regulate the formation and the dissociation of microfilament bundles *Biochem. J.* **288** 727–32
[33] Janmey P A 2001 Creating a niche in the cytoskeleton: actin reorganization by a protein kinase *Proc. Natl Acad. Sci. USA* **98** 14745–7
[34] Wong G C L *et al* 2003 Lamellar phase of stacked two-dimensional rafts of actin filaments *Phys. Rev. Lett.* **91** 018103
[35] Köhler O *et al* 2008 Rheological characterization of the bundling transition in F-actin solutions induced by methylcellulose *PLoS One* **3** e2736
[36] Medeiros N A *et al* 2006 Myosin II functions in actin-bundle turnover in neuronal growth cones *Nat. Cell Biol.* **8** 215–26
[37] Haviv L *et al* 2008 A cytoskeletal demolition worker: myosin II acts as an actin depolymerization agent *J. Mol. Biol.* **375** 325–30
[38] Kron S J and Spudich J A 1986 Fluorescent actin filaments move on myosin fixed to a glass surface *Proc. Natl Acad. Sci.* **83** 6272–6

[39] Raffel M, Willert C and Kompenhans J 1996 *Particle Image Velocimetry* (Berlin: Springer)
[40] Tawada K and Sekimoto K 1991 *J. Theor. Biol.* **150** 193–200
[41] Bischofs I B 2004 Elastic interactions of active cells with soft materials *Phys. Rev.* E **69** 021911
[42] Zemel A and Mogilner 2008 A Expansion and polarity sorting in microtubule-dynein bundles *Prog. Theor. Phys. Suppl.* **173** 17–25
[43] Zemel A and Mogilner A 2009 Physical Chemistry of Biomolecular Motors and Machine *Phys. Chem. Chem. Phys.* at press doi:10.1039/B818482H (Special issue)